Self-consistent cluster calculations of local magnetic properties of non-equilibrium crystalline FCC Cu-Fe and FCC Ag-Fe alloys

1992 J. Phys.: Condens. Matter 4 8813

(http://iopscience.iop.org/0953-8984/4/45/015)

J. Phys.: Condens. Matter 4 (1992) 8813–8822. Printed in the UK

Self-consistent cluster calculations of local magnetic properties of non-equilibrium crystalline FCC Cu–Fe and FCC Ag–Fe alloys

Cai Jian-Wang†, Luo He-Lie†, Zeng Zhi‡ and Zheng Qing-Qi‡

† State Key Laboratory of Magnetism, Institute of Physics, Academia Sinica, Beijing 100080, People's Republic of China

‡ Institute of Solid State Physics, Academia Sinica, Hefei 230031, People's Republic of China

Received 1 June 1992, in final form 15 July 1992

Abstract. The first-principles spin-polarized discrete variational X_α method was used to calculate the electronic structures at a central Fe site in a number of embedded clusters representing FCC Cu–Fe and FCC Ag–Fe alloys. The magnetic moment and isomer shift were derived from the calculations and compared with the existing experimental data. The calculated results show that the cluster model yields a magnetic moment and isomer shift consistent with experimental magnetization and Mössbauer data. The Fe 3d magnetic moment and isomer shift in Cu–Fe alloys decrease slightly on increase in the Cu concentration. The Fe 3d magnetic moment in Ag–Fe alloys is larger than that in Cu–Fe alloys. There is an enhancement of the magnetic moment in Ag–Fe alloys.

1. Introduction

In the equilibrium state, iron and copper have very small mutual solid solubilities and form no intermetallic compounds; neither do iron and silver. However, by using a vapour-quenching method such as sputtering, Cu–Fe and Ag–Fe solid solutions have been formed over the entire range of compositions [1–4]. These newly synthesized non-equilibrium crystalline alloys have recently been studied extensively. From the viewpoint of the crystalline structure, it has been found that both Cu–Fe and Ag–Fe alloys have a BCC structure at high Fe concentrations and an FCC structure at low Fe concentrations. Meanwhile, a large number of experimental data on their magnetic properties have been published. Fe_xCu_{1-x} solid solution is ferromagnetic in the range $x > 0.18$ regardless of its crystalline structure; when the Fe concentration is below 0.18, Cu–Fe alloys behave in a spin-glass-like manner. For BCC Cu–Fe alloys, the magnetic moment of the Fe atoms is nearly constant. For FCC Cu–Fe alloys, the magnetic moment of the Fe atoms monotonically decreases with increasing Cu concentration [2, 5]. As for the Fe_xAg_{1-x} solid solution, both the BCC and the FCC alloys are ferromagnetic with $x > 0.05$. A large Fe magnetic moment is found in FCC Ag–Fe alloys [4, 6]. All these magnetic properties are different from most cases in which the magnetic moment of the Fe atoms is quickly reduced by alloying with non-magnetic metals. Among the experimental techniques well suited to the study of local properties is Mössbauer spectroscopy, which allows measurement of

0953-8984/92/458813+10$07.50

the hyperfine interactions between the probe nucleus and its electronic environment. Chien *et al* [2] found that alloying with Cu causes the Fe isomer shift (IS) to increase, while Kataoka *et al* [7] observed that the ISS for FCC Ag–Fe alloys are insensitive to the alloying concentration.

Since these new materials were successfully synthesized, a large number of experimental data have been obtained. However, there seem to be hardly any theoretical studies on the local magnetic properties of non-equilibrium crystalline alloys yet. In the present work, we undertake an investigation of the electronic structure of FCC Cu–Fe and FCC Ag–Fe alloys by means of first-principles molecular cluster calculations within the framework of the discrete variational method, which has been applied to a significant number of cases and has been proved to be a powerful technique for studying the local effects [8–10]. We focus our attention on the electronic and magnetic properties at the central Fe sites in several possible atom configurations representing a series of alloys with different Fe concentrations, and hope to give a theoretical description of the alloying effect on local magnetic properties.

In the following section, we present the theoretical model used to calculate the electronic structure and the derived properties. In section 3, we present and discuss the results of our calculations and compare them with experimental data. Our conclusions are given in section 4.

2. Theoretical approach

Clusters with 19 atoms, as shown in figure 1, were used to calculate the electronic structures and other derived properties at the Fe site in the FCC Cu–Fe or FCC Ag–Fe alloys. In all these clusters, one Fe atom of special interest was located at the centre. Clusters with a Cu or an Ag atom taken as the central atom are not considered in this paper. The types of atoms in the first and second coordination shells are described in section 3. For comparison, we iterated a 15-atom cluster $FeFe_8Fe_6$, which has been used to describe the properties of α-Fe very well [8–12].

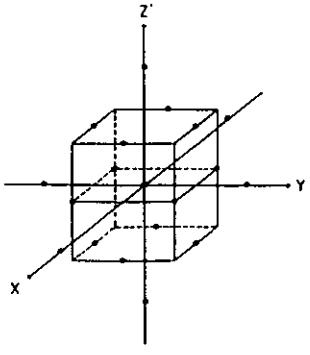

Figure 1. Representation of the 19-atom cluster for the FCC lattice.

Our calculations are based on the density-functional theory with the local-spin-density approximation, and a linear combination of atomic orbitals. A Hartree–Fock–Slater (HFS) X_α type of exchange–correlation function is used within the discrete

variational method. The same method has been employed in several other calculations on metal clusters [11, 12] and previously described in detail [13].

The non-relativistic one-electron Hamiltonian in the HFS model can be written in atomic units as

$$h_\sigma = -\tfrac{1}{2}\nabla^2 + V_{\text{Coul}}(\rho_\sigma) + V_{\text{xc}}(\rho_\sigma).$$

The Coulomb potential $V_{\text{Coul}}(\rho_\sigma)$ includes both electron–electron and electron–nuclei interactions. The spin-dependent exchange–correlation potential $V_{\text{xc}}(\rho_\sigma)$ was chosen to be of the spin-polarized von Barth–Hedin [14] form. The electronic density ρ_σ for each spin σ is given by

$$\rho_\sigma(r) = \sum_i n_{i\sigma}|\Phi_{i\sigma}(r)|^2$$

where $n_{i\sigma}$ is the occupation of the cluster spin orbital $\Phi_{i\sigma}$, determined by Fermi–Dirac statistics. The molecular spin orbitals $\Phi_{i\sigma}$ are expanded as a linear combination of numerical symmetrized atomic orbitals.

The atomic basis set of the form $R_{nl}Y_{lm}(\theta, \varphi)$, with $R_{nl}(r)$ the numerical radial functions, are the orbital solutions of the self-consistent-field Schrödinger equation for Fe, Cu and Ag atoms in spherical potential wells. In the variational expansion of the cluster spin orbitals $\Phi_{i\sigma}$, the numerical atomic orbitals 3s, 3p, 3d, 4s and 4p for central Fe are included. For Cu and other Fe, only the 3d, 4s and 4p orbitals are kept in the variational basis; for Ag the 4d, 5s and 5p orbitals are included. The remaining low-lying orbitals are used to build the potential but are frozen after the first cycle in all cases. The valence orbitals are orthogonalized with respect to the core.

The secular equations $(\mathbf{H} - E\mathbf{S})\mathbf{C} = 0$ are finally solved self-consistently, using matrix elements determined by numerical integration on a random-point grid by the diophantine method [13].

The actual electronic density is replaced by a model density $\rho_\sigma^{\text{SCC}}(r)$, which is a superposition of the radial densities R_{nl}^ν centred on cluster atoms via the diagonal-weighted Mulliken population f_{nl}^ν. The potential used in this work is derived from this density, which is the so-called self-consistent charge (SCC) approximation:

$$\rho_\sigma^{\text{SCC}} = \sum_{nl}\sum_\nu f_{nl}^\nu |R_{nl}(r_\nu)|^2.$$

Finally, an embedding scheme [13] is employed to simulate the effect of the rest of the microcrystal on the cluster, i.e. all the clusters are embedded in the Cu–Fe or Ag–Fe microcrystal which is the periodic translation of the corresponding cluster; it consists basically of placing numerical atomic potentials at about 300 closeted sites surrounding the cluster. The embedding potentials are derived from superposition of the electronic densities of atoms placed at the crystal sites exterior to the cluster. These potentials are truncated by means of a pseudopotential to simulate the orthogonality effect. In order to make the comparison reliable, all the input parameters underwent no change, such as the atomic basis functions, integration points and crystal potentials.

The IS in Mössbauer spectra can be related to the difference between the electronic densities at the nuclei between the source and absorber, which is given by

$$\text{IS} = \alpha[\rho_{\text{A}}(0) - \rho_{\text{S}}(0)]$$

where α is a calibration constant which includes terms due to nuclear radii changes and relativistic effects. We took $\alpha = -0.25a_0^3$ mm s^{-1} which is close to a recent estimate [15]. Our calculation for the IS did not include the contributions from the deep-core 1s and 2s orbitals of Fe since the computed difference between $\rho(0)$ for these orbitals in different environments is negligible [8].

3. Results of calculations and discussion

Since the centre atom in a cluster has complete nearest- and next-nearest-neighbour shells, we believe that it describes the properties of the bulk solid better than those atoms in the outer coordination shells do; this has been confirmed by many calculations on metallic clusters [8–10]; thus the electronic structures and derived properties of the central Fe site in the embedded cluster are investigated in this paper. There are various locations of nearest-neighbour Fe atoms; we considered only the most probable configuration with the highest symmetry, i.e. the following cases: FeM_3 (M ≡ Cu or Ag), represented by the cluster $FeM_{12}Fe_6$ in O_h symmetry; Fe_3M_5, represented by the cluster $Fe(Fe_2M_{10})Fe_6$ in D_{2h} symmetry; FeM, represented by the cluster $Fe(Fe_4M_8)Fe_6$ in D_{2d} symmetry.

3.1. Results for FCC Cu–Fe alloys

3.1.1. Magnetic moment. In FCC Cu–Fe alloys the lattice constants hardly change with concentration [2]; we assumed that no local distortion was present when the Fe atom substitutes for the Cu atom in the FCC Cu geometry. In our calculations, the lattice parameter of FCC Cu–Fe alloys is 3.61 Å. In table 1 the local magnetic moments, including the calculated values and experimental data, are given.

Table 1. Local magnetic moments and d charges for FCC Cu–Fe alloys.

			Central Fe				NN Cu	Fe	
Alloy	Cluster	Symmetry	μ_{3d} (μ_B)	μ_{4s+4p} (μ_B)	μ_{total} (μ_B)	d charge	μ_{total} (μ_B)	atom moment	
α-Fe	$FeFe_8Fe_6$	O_h	3.11	−0.31	2.80	6.28		2.2	[5]
FeCu	$FeFe_4Cu_8Fe_6$	D_{2d}	3.26	0.06	3.32	6.31	−0.31	2.1	[5]
Fe_3Cu_5	$FeFe_2Cu_{10}Fe_6$	D_{2h}	3.23	0.09	3.32	6.26	−0.12	1.7	[5]
$FeCu_3$	$FeCu_{12}Fe_6$	O_h	3.17	0.10	3.27	6.22	−0.06	1.4	[5]
Dilute Fe–Cu	$FeCu_{12}Cu_6$	O_h	3.41	0.20	3.61	6.33	0.05	3.68	[17]

As noted before, there is a finite cluster effect because the overlap of orbital wavefunctions in the cluster is not so complete as that in the bulk solid; thus, the calculated magnetic moment using the molecular cluster method is usually larger than the value for bulk solid materials [8, 9]. In table 1, we find that the total magnetic moment for the pure iron cluster, 2.80 μ_B, is significantly larger than the experimental value of 2.2 μ_B. The study on the convergence of the magnetic moment to a bulk value by Press *et al* [11] shows that the magnetic moment of the central atom in a cluster of 27 Fe atoms approaches the bulk value. It can be concluded that the cluster with one or two more shells will reproduce the bulk value very well but, accordingly, it is computationally expensive. For most physical properties, it has been justified

that the three- to four-atom-shell cluster is sufficient [8, 11] and, for the magnetic moment of the alloys, one can focus on trends instead of absolute values. Such a treatment is not only computationally attractive but also physically reasonable. The situation for describing the magnetic moment at very dilute concentrations is better because of its more localized characterization. Guenzburger and Ellis [8] found that the calculated magnetic moment of Ti impurities in Fe was in very good agreement with the measured value.

From table 1, it is noted that the central Fe 3d magnetic moments of all the Cu–Fe alloys are larger than that of α-Fe, which may result from the environment difference between the 19-atom cluster and the 15-atom cluster.

By analysing table 1, it may be seen that there is a large positive 3d magnetic moment of Fe atoms for our calculated cases, which shows that these Cu–Fe alloys are ferromagnetic. The 3d moment of the central Fe atom decreases with decreasing Fe substitutions in the nearest-neighbour shell. In table 1 it is noted that there is a negative magnetic moment with the Cu atom in FCC Cu–Fe alloys. The Fe 4s+4p magnetic moment is negative in pure iron and becomes positive in Cu–Fe alloys. This could be because the s and p electrons interact antiferromagnetically with the d electrons on neighbouring atoms, as pointed out first by Anderson and Clogsten [16]. In pure iron, all d moments are pointing up; s–d and p–d interactions result in a negative 4s+4p moment. With the appearance of Cu atoms in the first shell the 4s+4p moment at the Fe site starts to change direction since the moment on Cu is negative.

As the experimental data on the magnetic moment of Fe atoms in Cu–Fe alloys were obtained on the assumption that Cu atoms carry no magnetic moment [5], and almost all the magnetic moment of Cu–Fe alloys comes from the Fe 3d moment, the varying trend in the Fe 3d magnetic moment, instead of the absolute value of the Fe atom total magnetic moment, should be taken care of here. From this point of view, the calculated Fe 3d magnetic moment, which tends to decrease with increasing Cu concentration, is consistent with the measurements of Sumiyama *et al* [5], shown in table 1.

If we consider the 3d charge in table 1, we can observe that it decreases with decreasing Fe substitutions in the nearest-neighbour shell; this may be considered to be one of the reasons for a smaller local magnetic moment with increasing Cu concentration in FCC Cu–Fe alloys. Further discussions will follow with the help of an analysis of the local densities of states (DOSS) and ISS.

From table 1, there is a large local magnetic moment in the dilute alloy of Fe in Cu, even larger than magnetic moments of all other FCC Cu–Fe alloys. We consider that the Fe atom in this local environment is more atomic like. The calculated value is in fairly good agreement with the experimental data of Hurd [17] for a dilute alloy of Fe in Cu. The molecular embedded-cluster model, based on the local-density-functional approximation, can be used to treat localized defects in solids very effectively.

3.1.2. Density of states. Figure 2(*a*) shows the central Fe 3d DOS of the 15-atom cluster representing α-Fe; figures 2(*b*)–2(*d*) depict the local density of 3d states for the central Fe atom in three cluster environments representing the Cu–Fe alloys with different Fe atom concentrations.

The local DOS is defined here in terms of the Mulliken population as

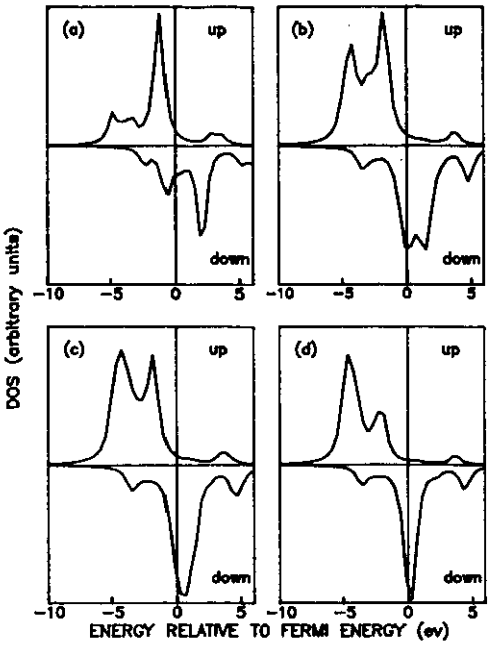

Figure 2. Local DOSS for the central Fe 3d majority spin (up) and minority spin (down): (a) $FeFe_8Fe_6$; (b) $FeFe_4Cu_8Fe_6$; (c) $FeFe_2Cu_{10}Fe_6$; (d) $FeCu_{12}Fe_6$. The spin-up and spin-down bands are normalized to the same scale within each cluster.

$$D^{\nu}_{nl}(E) = \sum_{p} f^{\nu}_{nl,p} \frac{\sigma/\pi}{(E-\epsilon_p)^2+\sigma^2}$$

where $f^{\nu}_{nl,p}$ is the population contribution to the molecular orbital p corresponding to the energy ϵ_p. The Lorentzian width parameter σ was chosen to be 0.1 eV.

From these diagrams, some general features can be observed as increasing the number of Cu nearest neighbours, i.e. increasing the Cu concentration in Cu–Fe alloys.

(1) The two larger 3d peaks for minority-spin states tend to collapse into a single broad peak, and finally a sharp single peak near the Fermi level grows. The minority-spin 3d peaks above the Fermi energy move towards the Fermi level. As a result, the 3d local magnetic moment decreases with increasing number of Cu nearest neighbours, which can be the other reason except for the decrease in Fe 3d charge.

(2) For majority-spin states, the small peak at a low energy becomes larger and meanwhile the main peak near the Fermi level becomes smaller until finally the main peak is at the lower-energy position. Thus, in the sense of the Fermi surface relating to the 3d band, alloying Fe in Cu causes Fe atoms to change from weakly ferromagnetic to strongly ferromagnetic, which is completely different from the cases of alloying Fe in Al, Si, etc [9, 12].

We also calculated the 3d DOS of the metal Cu represented by the cluster $CuCu_{12}Cu_6$, as shown in figure 3(*a*), which closely resembles the result of band calculations [18]. Figure 3(*b*) is the 3d DOS of FeCu obtained by summing over the majority-spin states and minority-spin states. The results depicted in figures 3(*a*) and 3(*b*) indicate that the Fe 3d states are above the Cu 3d states, which is in agreement with the XPS measurement [2]. Such band structures make the Cu 3d band mainly affect the lower half of the Fe 3d band which is almost occupied by the majority-spin electrons; this results in the strong ferromagnetism of Fe atoms in Cu–Fe alloys.

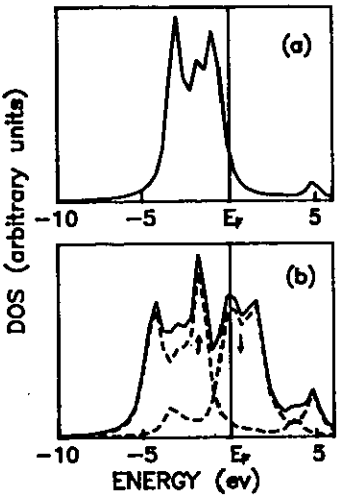

Figure 3. (*a*) 3d DOS of metal Cu by calculating the cluster $CuCu_{12}Cu_6$. (*b*) 3d DOS of FeCu with the full curve representing the sum of the majority-spin states and minority-spin states, and the broken curves representing the spin-up (↑) and spin-down (↓) bands, respectively.

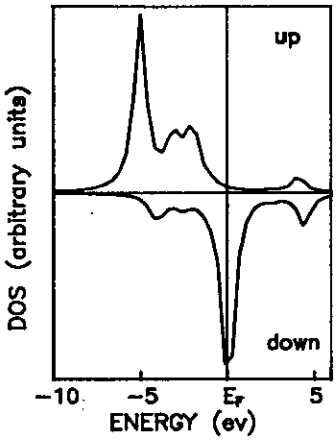

Figure 4. 3d DOS of dilute Fe in Cu.

On the other hand, most of the states just above the Fermi level are the Fe 3d minority-spin states. When the Cu 4s and 4p states interact with the Fe 3d states, they form bonding and antibonding hybrids; the bonding hybrids lie in the filled valence region, and the antibonding hybrids lie above the Fermi energy. To accommodate the total charge, some charge is accommodated in empty states near the Fermi energy which are mainly minority-spin states. Such an interaction leads to a decrease in the minority-spin peaks, making Cu atoms have a negative magnetic moment in the Cu–Fe alloys.

In figure 4, the DOS of dilute Fe in Cu is drawn. Clearly, the main 3d peaks of majority spin and minority spin are both very sharp; it is seen that the Fe atom in the alloy has an 'isolated-atom' behaviour. The atomic-like nature of Fe in the alloy would account for its enhanced magnetic moment.

3.1.3. Isomer shift. The calculated IS values at the central Fe site, which are relative to α-Fe, are listed in table 2.

Table 2. Calculated IS of Cu–Fe clusters and the measured IS values for Cu–Fe alloys. n_{4s} is the Mulliken population for the 4s orbital, $\rho(0)$ is the 3s+valence charge density at the central Fe atom. $\alpha = -0.25\ a_0^3$ mm s^{-1} was used to calculate the IS.

Cluster	4s charge n_{4s}	$\rho(0)$ (units of a_0^{-3})	IS (mm s^{-1})	
			Calculated	Experimental [2]
$FeFe_8Fe_6$	0.74	146.687	0	0
$FeFe_2Cu_{10}Fe_6$	0.70	146.035	0.163	0.13
$FeFe_4Cu_8Fe_6$	0.57	145.999	0.172	0.15
$FeCu_{12}Fe_6$	0.52	145.942	0.186	0.16

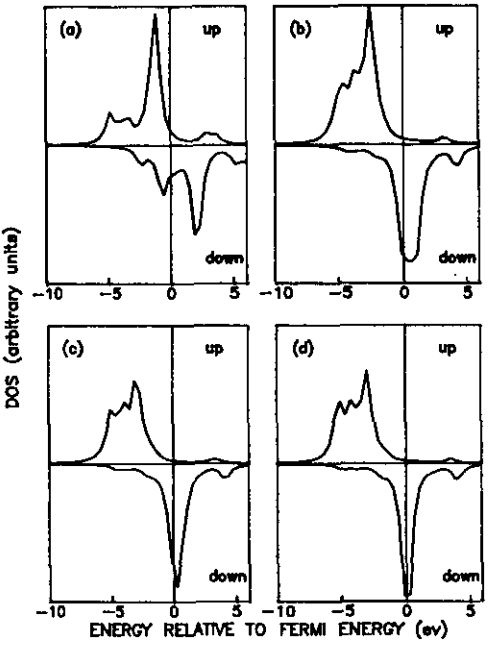

Figure 5. Local DOSs for central Fe 3d majority spin (up) and minority spin (down): (a) $FeFe_8Fe_6$; (b) $FeFe_4Ag_8Fe_6$; (c) $FeFe_2Ag_{10}Fe_6$; (d) $FeAg_{12}Fe_6$.

From table 2 it can be seen that the charge transfer seems to play an important role in the properties of the Cu–Fe alloys; of course, only s-electron transfer can be measured by the IS method. It is noted that the ISs are positive values for FCC Cu–Fe alloys, which means that charge transfer from Fe valence orbitals into the Cu neighbours takes place, as can be expected owing to the difference in their Pauling electronegativities: Fe, 1.8; Cu, 2.0. From table 2, it can be seen that the IS increases as increasingly fewer Fe atoms substitute for Cu atoms. Our calculated results are in good agreement with the Mössbauer studies of Chien *et al* [2]. For all these cases, the 4s Mulliken populations in table 2 are observed to have the same tendency as the IS; the number of electrons transferred at the central Fe site increases with increase in the Cu concentration.

In summarizing the relationship between the Pauling electronegativities and the Mulliken 3d and 4s populations, which are shown in table 1 and table 2, respectively, it should be pointed out that the present investigation does not agree with what Watson and Bennett [19] concluded; our calculation on Fe–Cr clusters did agree, however [20]. Instead of the opposite varying tendency of the 4s electron and the 3d electron in metal alloys or intermetallic compounds, a 4s electron transfer from the Fe atom to the Cu atom occurs; in the meantime, the number of 3d electrons of the Fe atom decreases. Such a case might arise because copper and iron form no intermetallic compounds in the equilibrium state; Cu–Fe alloys can exist only in a non-equilibrium crystalline state.

3.2. Results for FCC Ag–Fe alloys

The electronic configurations of Ag atoms resemble those of Cu atoms. However, the radius of the Ag atom is larger than that of the Cu atom, and so is the crystalline parameter of Ag. The non-equilibrium Ag–Fe alloys are found to change their lattice

constants linearly with concentration in the range of the FCC phase [6]. We calculated the properties of the FCC Ag–Fe alloys by the same method as presented above.

3.2.1. Magnetic moment. For FCC Ag–Fe alloys, the calculated magnetic moments, including their lattice constants, are listed in table 3.

Table 3. Calculated local magnetic moments of FCC Ag–Fe alloys.

				Central Fe				NN Ag
Alloy	Cluster	Lattice constant (Å)	Symmetry	μ_{3d} (μ_B)	μ_{4s+4p} (μ_B)	μ_{total} (μ_B)	d charge	μ_{total} (μ_B)
FeAg	$FeFe_4Ag_8Fe_6$	3.986	D_{2d}	3.55	0.19	3.74	6.26	−0.27
Fe_3Ag_5	$FeFe_2Ag_{10}Fe_6$	4.018	D_{2h}	3.53	0.18	3.71	6.28	−0.18
$FeAg_3$	$FeAg_{12}Fe_6$	4.036	O_h	3.54	0.20	3.74	6.32	−0.16

In table 3 it is found that the magnetic moment of the central Fe site is very large, much larger than that in FCC Cu–Fe alloys; such a comparison rules out the cluster size effect. Therefore, there is an enhanced magnetic moment in FCC Ag–Fe alloys in the range of concentrations studied; this is consistent with the magnetic measurements of Kataoka *et al* [4]. The local magnetic moment of the central Fe atom hardly varies with the number of nearest Ag neighbours in our study range. Because of the random distributions of the experimental data in this range, further comparison with the existing experimental data is not practicable.

As shown in table 3, the Fe 4s+4p magnetic moment has a positive value, but the moment of Ag atoms is negative in FCC Ag–Fe alloys. This may result from the same physical mechanism as in FCC Cu–Fe alloys.

3.2.2. Density of states. Figures 5(*a*)–5(*d*) depict the Fe 3d DOSS for α-Fe, FeAg, Fe_3Ag_5 and $FeAg_3$ alloys, respectively. From these diagrams, we can observe the features of FCC Ag–Fe alloys as follows.

(1) For minority-spin states, compared with that of α-Fe, the low-energy 3d peak disappears, the two larger 3d peaks collapse into a single peak near the Fermi surface, and this peak becomes sharper with increasing number of nearest Ag neighbours.

(2) For majority-spin states, while there is a decrease in the main peak, the small peak at the low-energy position grows.

In other words, the energy splitting between the main (majority-spin and minority-spin) 3d peaks for Ag–Fe clusters is wider than that for Cu–Fe clusters with similar shell structures, and the band width for the former is smaller than that for the latter; this is due, on the one hand, to the larger lattice constants in the FCC Ag–Fe alloys than in the FCC Cu–Fe alloys and, on the other hand, to the lower d band in Ag metal than in Cu metal [18]. All these factors result in a much larger local magnetic moment for FCC Ag–Fe alloys than for FCC Cu–Fe alloys.

4. Conclusions

The spin-polarized discrete variational method in the local-density approximation has been employed to obtain the electronic structures at a central Fe site in a number of

embedded clusters representing FCC Cu–Fe and FCC Ag–Fe alloys. The local magnetic moment and IS were derived from the calculations and compared with the existing experimental data.

(1) For FCC Cu–Fe alloys, the Fe 3d magnetic moment and IS decrease slightly with increasing Cu concentration. The tendency of the magnetic moment to vary is consistent with the magnetic measurement results. Our calculated results are in good agreement with the Mössbauer IS and XPS data. On the basis of a DOS and charge transfer analysis, the magnetic moment and IS have been explained reasonably.

(2) For FCC Ag–Fe alloys, calculations show that there is an enhanced magnetic moment for Fe atoms, except, of course, for the cluster size effect. The large Fe atom magnetic moment is ascribed to the wider energy splitting between the main majority-spin peak and the main minority-spin peak in the DOS, and the narrowing of the Fe 3d band width.

Acknowledgments

This work was performed on the DEC-5000, in the Institute of Physics, Academia Sinica.

References

[1] Sumiyama K and Nakamura Y 1983 *J. Magn. Magn. Mater.* **35** 219
[2] Chien C L, Liou S H, Kofalt D, Yu Wu, Egami T and McGurie T R 1986 *Phys. Rev.* B **33** 3247
[3] Chien C L and Unruh K M 1983 *Phys. Rev.* B **28** 1214
[4] Kataoka N, Sumiyama K and Nakamura Y 1985 *J. Phys. F: Met. Phys.* **15** 1405
[5] Sumiyama K, Yoshitake T and Nakamura Y 1984 *J. Phys. Soc. Japan* **53** 3160
[6] Kataoka N, Sumiyama K and Nakamura Y 1988 *J. Phys. F: Met. Phys.* **18** 1409
[7] Kataoka N, Sumiyama K and Nakamura Y 1985 *Trans. Japan Inst. Met.* **26** 703
[8] Guenzburger D and Ellis D E 1985 *Phys. Rev.* B **31** 93
[9] Chacham H, Galvão da Silva E, Guenzburger D and Ellis D E 1987 *Phys. Rev.* B **35** 1602
[10] Guenzburger D, Ellis D E and Danon J A 1986 *J. Magn. Magn. Mater.* **59** 139
[11] Press M R, Liu F, Khanna S N and Jena P 1988 *Phys. Rev.* B **40** 399
[12] Li Z Q, Luo H L, Lai W Y and Zheng Q Q 1991 *J. Phys.: Condens. Matter* **3** 6649
[13] Ellis D E 1968 *Int. J. Quantum Chem. Symp.* **2** 35
Ellis D E and Painter G P 1970 *Phys. Rev.* B **2** 2887
[14] von Barth U and Hedin L 1972 *J. Phys. C: Solid State Phys.* **5** 1629
[15] Duff K J 1974 *Phys. Rev.* B **9** 66
[16] Anderson P W and Clogsten A M 1961 *Bull. Am. Phys. Soc.* **6** 124
[17] Hurd C M 1967 *J. Phys. Chem. Solids* **28** 1345
[18] Muruzzi V L, Janak J F and Williams A R 1978 *Calculated Electronic Properties of Metals* (Oxford: Pergamon)
[19] Watson R E and Bennet L H 1978 *Phys. Rev.* B **18** 6439
[20] Li Z Q and Luo H L 1991 *J. Phys.: Condens. Matter* **3** 9141